TECHNICAL ARTICLE

Process Optimization and Characterization of Ultra-Thin Dissimilar Sheet Material Joints for Battery Applications Using Ultrasonic Welding

Aru Ranjan Singh, Coomar Sudarsan, Abhishek Das, Sumit Hazra, and Sushanta Kumar Panda

The present work explored the application of ultrasonic welding process for an acceptable robust joint of dissimilar ultra-thin sheet materials. The joining process was carried out with two material combinations for potential battery application, and these were aluminum (grade AA1050) of 0.2 mm thickness with copper (grade C101S) of 0.3 mm thickness and C101S with nickel-coated steel of 0.3 mm thickness. The input parameters affecting the weld quality were identified, and the optimization of these parameters was carried out through response surface methodology to maximize the output responses of lap shear and T-peel strength. The cross section of weld samples was characterized using optical microscopy, SEM and micro-hardness tests in order to understand the bond mechanism. It was observed that the bond strength was a combination of metallurgical bonding, mechanical interlocking and inter-metallic diffusion. Higher hardness was found in the region where the sonotrode tip contacted the sample, indicating excessive plastic deformation. However, the hardness near the valley region was similar or lower compared to the hardness of parent material due to heat generation and subsequent thermal softening. The strength and microscopy characterization data were used to establish a relationship between the mode of failure and the physical attributes of the weld.

1. Introduction

In the present-day scenario, the strict government norms regarding the climate change and the depletion of fossil fuels have led to an increase in the use of the battery sourced electric vehicles. The efficiency and lifetime of the electric vehicles are largely dependent on the battery pack that is being used for the generation of the energy source. The battery pack is a combination of individual cells electrically connected to each other with the help of tabs and bus bar (Ref 1-3). These cells are contained structurally inside a purpose-built module to enhance the power output. A typical cell is fabricated in various shapes and sizes and is assembled in different configurations to form a module inside the battery pack. Therefore, the battery pack consists of combination of materials with different properties and thicknesses intended for a particular functionality. The efficiency of the battery pack can be increased with the decrease in the overall weight of the battery which in turn can

be done with the use of ultra-thin sheets (Ref 1). The fabrication of the battery module therefore involves the permanent joining of different ultra-thin sheets based on their applications inside the module. However, the joining in case of a battery module involves joining of highly conductive and dissimilar materials such as pure copper to commercially available pure aluminum. These materials can have different thicknesses which can impact the mechanical strength of the joint. Also, during the service of the battery pack, these joints are expected to sustain the harsh environment that includes being subjected to vibration, unpredictable weather conditions and impact. The joining of thin sheets through the process of traditional fusion welding processes like TIG welding, laser welding, electron beam welding and solid-state joining process have been well developed previously. The major drawbacks of the conventional fusion welding process include the formation of porosity and cracks in the weld and the formation of intermetallic compounds which decrease the weld strength. More broadly, the formation of a larger weld nugget process makes it unsuitable for welding of highly conductive materials during battery pack manufacturing. These factors limit the application of fusion welding process for the joining of the components in case of battery module (Ref 2).

The present work will explore the feasibility of ultrasonic welding (UW) as a method for the joining of these battery components because of its advantages over the fusion welding methods. The ultrasonic welding occurs without melting of the materials. As a result, it does not require any filler materials and is able to maintain higher joint strength (Ref 2-6). This characteristic property makes UW an effective welding process for dissimilar (Ref 2, 4, 5) and ultra-thin (Ref 4) materials as the process does not develop large amount of heat during the

Aru Ranjan Singh, Abhishek Das, and **Sumit Hazra**, Warwick Manufacturing Group, University of Warwick, Coventry CV4 7AL, UK; and **Coomar Sudarsan** and **Sushanta Kumar Panda**, Department of Mechanical Engineering, Indian Institute of Technology, Kharagpur, West Bengal 721302, India. Contact e-mail: sushanta.panda@mech.iitkgp.ac.in.

welding process. During the UW process, a high frequency oscillation is created in a 'sonotrode' by a piezoelectric transducer. This oscillation combined with pressure that is applied through the sonotrode causes the atoms on the metal surface to bond without melting the material. It particularly happens because the high pressure and friction forces generated during the process breaks down the surface oxide layer on the aluminum to form a bond with the substrate (Ref 7). Therefore, UW is regarded as a flexible process for joining of conductive and dissimilar ultra-thin sheet materials such as copper and aluminum.

Although the UW process possesses distinctive advantages over the other fusion and solid-state welding process, the mechanism of bond formation and the characterization of the quality of the weld that is formed is still under research for its mass application in the battery manufacturing. There have been a few investigations regarding the bond mechanism and the quantification of the weld quality, but a more detailed study is required in case of the welding of dissimilar ultra-thin sheets. During the welding of dissimilar conductive materials, the clamping pressure and welding time were considered as the input factors, and it was observed that metallurgical adhesion and mechanical inter-locking were the main reasons for the formation of the bond during the ultrasonic welding process (Ref 4). The joining of aluminum and stainless-steel foils was carried out, and the welded joints were investigated to understand the effect of welding parameters on microstructure and mechanical properties. The above study correlated the physical attributes such as bond density and post-weld thickness with the quality of the joints (Ref 5). In another study, a three-dimensional finite element model was developed to simulate the coupled thermal-mechanical fields in the UW of aluminum foils (Ref 7). It was observed that severe localized plastic deformation at the bond region was the major phenomena for the bond formation. The welding mechanism of the Al/Cu ultra-thin sheets was studied through microstructural analysis, and it was reported that the primary mechanism for joining was due to the mechanical intermixing (Ref 8). Further, through another study it was identified that the metallurgical bonding was the primary cause for the bonding in case of the ultrasonic joining process, and it was found that the removal of surface oxide layer helped in bond formation (Ref 9). However, in case of Al-Cu ultrasonic joint, inter metallic diffusion was observed during the investigation of the effect of welding energy on the weld quality (Ref 10). Similarly, in another Al-Cu ultrasonic joint study, it was found that mechanical interlocking and inter-diffusion were the reasons for the weld formation (Ref 11). It can be observed that investigations were carried out in order to understand the bond mechanism, however it was difficult to provide a conclusive remark on the exact principle of bond formation in case of the dissimilar welding of ultra-thin sheets.

In order to ensure high mechanical strength, the UW process requires a careful selection of the input parameters. The previous studies on the welding of the ultra-thin sheets reported that the welding time, pressure, amplitude of vibration, welding power were the parameters that affected the weld quality and strength (Ref 12). The effect of the input parameters such as welding time and welding pressure was studied during the welding of Cu-Ni foils, and the sensitiveness of these parameters to T-peel strength of the joints was successfully demonstrated (Ref 13). The welding pressure, amplitude of vibration and welding time were considered as input parameters

and lap shear and T-peel strength as output responses during the joining of copper with multiple layers of aluminum (Ref 14). The effect of the individual parameter on the output responses was investigated keeping the other parameters constant. It was observed that with the increase in the amplitude and welding time, the lap shear strength initially increased, attained an optimum value, and finally decreased. However, the T-peel strength increased with the increase in the amplitude and welding time.

Several statistical methods are available such as factorial method, Taguchi method, response surface methodology (RSM) to develop mathematical models so as to optimize the input parameters. RSM is a suitable optimization method as compared to other techniques as it requires a smaller number of experimental trials (Ref 15, 16). Several investigations have been carried out using RSM as an effective tool for the optimization of the process parameters in joining processes (Ref 17). A response surface methodology was used to optimize the ultrasonic joining process parameters such as pressure, temperature and welding time for aluminum to copper multilayer joints where a complex nonlinear behavior of input parameters on the lap shear and T-peel strength was observed (Ref 18). It was also noted that both lap shear and T-peel strength increased simultaneously until the lap shear strength reached the maximum value before decreasing with incremental increase in T-peel load.

Despite the extensive research on ultrasonic joints of dissimilar materials such as between magnesium alloy (Ref 19), Cu and Ni foils (Ref 20), steel and Al (Ref 21), Al and Cu (Ref 22), and zinc with Al (Ref 23), there is no detailed joining analysis and optimization reported in literature that considers thin copper to steel and aluminum to copper joints using UW. Therefore, in the present study, an attempt was made to investigate the joining process of different ultra-thin dissimilar materials with varying thickness to establish the robustness of the UW process. The effect of input parameters such as welding pressure, amplitude of sonotrode vibration and welding time on weld properties such as the joint strength was investigated by using the design of experiment methodology. The weld strength was measured through T-peel and lap shear tests, and the welding process was monitored in-situ with thermal measurements and ex-situ with hardness measurements. The relationship between weld strength and process input parameters was analyzed with the response surface method to identify the range of optimal process parameters. The optimization of these input parameters was carried out using the RSM technique. This was supplemented with microstructural observations of the weld cross sections in order to identify the mechanism of bond formation in the dissimilar material welding. The developed statistical model correlating the lap shear and peel strengths with amplitude of sonotrode vibration, welding pressure and welding time will provide guidelines to manufacturing and materials engineers for getting better dissimilar material joint for battery applications.

2. Materials and Methods

2.1 Materials Selection

The battery pack is a combination of individual cells electrically connected to each other with the help of tabs and

bus bar as mentioned previously. In battery pack, two welds are applied, firstly between battery casing and the tab terminal and secondly between tab terminal and bus bar. Ultra-thin sheets of aluminum and copper material can be used as battery tabs and bus bar, respectively, because of their superior electrical and thermal conductivity (Ref 24, 25). The battery casing is also an important part in battery pack manufacturing, and the casing must have higher strength, ductility and better corrosion resistance. In this regard, Ni-coated steel is generally used for the casing as the Ni-coating gives an excellent chemical resistance and wear resistance property to the steel (Ref 26). Therefore, in the present work, commercial pure copper (C101S), aluminum (AA1050 H14, and it has been referred as AA1050), Ni-coated steel of thickness 300 μm, 200 μm and 300 μm, respectively, were considered.

The chemical compositions of the three ultra-thin sheet materials are listed in Table 1. Uniaxial tensile tests were carried out in order to evaluate mechanical properties such as the ultimate tensile strength (UTS), yield stress at 0.2% offset, strain hardening exponent (n-value), elongation and the normal plastic anisotropy ratio ($\bar{r}$) of the individual materials. The tests were carried out on a universal tensile testing machine using the standardized samples prepared according to ASTM E8 standard as mentioned elsewhere (Ref 27). The measured mechanical properties are also enlisted in Table 1.

2.2 Design of Experiments

The ultra-thin sheets were used for the welding experiment in two material and thickness combinations i.e., (1) AA1050 (200 μm) with C101S (300 μm) (Al-Cu), and (2) C101S (300 μm) with Ni-coated steel (300 μm) (Cu-Steel). In order to determine the optimal parameters for each joint combination, the design of experiment method was first used to model the effect of process parameters on weld quality. The response surface method was then used to identify the optimal process settings for welding these materials. The RSM is a combination of statistical and mathematical techniques, and it is widely used to optimize and improve the welding conditions in order to generate successful welds (Ref 17, 18, 28). The main objective is to find an optimal set of operating parameters to create the welds required for each combination of materials. In this kind of problem, the relationship between responses i.e., the output variables and parameters are unknown, therefore, first experimental data are gathered then the data are fitted with series of nonlinear polynomial models to create a response surface. The optimal process parameters were identified through the topology of RSM. The fitting of the response surface effectively in

RSM requires a good set of experiments, therefore, the design of experiment (DOE) helps in choosing the appropriate number of experiments within the specified process window. Among the different DOE techniques, the central composite design (CCD) is the most widely used technique for modeling of welding processes (Ref 15, 16). This is because the CCD is relatively efficient with respect to the number of runs required. The CCD generated response surface can rapidly and effectively move close to the optimum; hence, this technique was used in the present study (Ref 16). In order to carry out the DOE, three input parameters i.e., welding time (t), amplitude of sonotrode vibration (A) and welding pressure (p) were considered based on their effect on the strength of the weld post the ultrasonic welding process. The output strength responses were taken as the lap shear load (F_{shear}) and T-peel load (F_{peel}) of the welded materials. In order to decide the range of input parameters, a small-scale pilot run was conducted.

Pilot experiments were carried out to identify the upper and lower limits. The lower limits of parameters were determined by examining the quality of the weld formed through hand peeling. The higher limits were identified by visually inspecting the welds and assessing its quality for material penetration and absence of visual defects. The design of the CCD is shown in Table 2. Five level of parameters were chosen for the CCD to generate 20 experiments with six central points. The analysis of the results was carried out by using Design Expert 12 software. In this study, four repetitions were done; therefore, a total of eighty experiments were carried out for each configuration (i.e., lap shear and T-peel) and each material combination (i.e., Al-Cu and Cu-Steel). The averaged-out values were taken to fit the response and the factors in the RSM.

2.3 Welding Procedure

The schematic of ultrasonic welding (UW) process and the machine set-up head used in the present work are shown in Fig. 1(a) and (b). The joining of the ultra-thin sheets was carried out using a Telsonic MPX ultrasonic welding system having a clamping force range up to 5 kN and peak power of 6.5 kW. The range of clamping force and power provides the flexibility to carry out the design of experiment mentioned in Table 2. In the present work, the ultrasonic welding frequency was kept constant at 20 kHz.

The horn of the welding setup was made up of titanium alloy, whereas the anvil was fabricated from steel. The ultra-thin sheets were clamped in between the horn and the anvil in order to produce the welds. The serrations on the top of the anvil ensured the non-sliding of the ultra-thin sheets, whereas

Table 1 Chemical composition and mechanical properties of the ultra-thin sheets

Material	Chemical composition, wt.%	0.2% YS, MPa	UTS, MPa	n	K, MPa	$\bar{r}$	% Elongation
AA1050 (200 μm)	Si < 0.25, Fe < 0.40, Cu < 0.05, Mn < 0.05, Mg < 0.05, Zn < 0.07, Ti < 0.05, Al-balance	118	120	0.12	200	0.73	6.31
C101S (300 μm)	Cu > 99.99, O < 0.0005, other-balance	78	350	0.44	488	0.72	52
Ni-coated low carbon steel (300 μm)	C < 0.047, Mn < 0.235, P < 0.011, S < 0.01, Al < 0.059, Si < 0.002, B < 0.0019 Fe-balance	182	459	0.26	477	1.09	38

Table 2 Domain of process parameters for different welding material and parameter combinations

Weld combination	Variables	Levels				
		−1.682	−1	0	1	1.682
Al-Cu	Welding pressure, p, bar	0.59	1.2	2.1	3	3.61
	Welding time, t, sec	0.15	0.25	0.4	0.55	0.65
	Amplitude, A, μm	30	35	42.5	50	55
Cu-Steel	Welding Pressure, bar	1.39	1.8	2.4	3	3.41
	Welding Time, sec	0.21	0.3	0.425	0.55	0.64
	Amplitude, μm	40	43	47.5	52	55
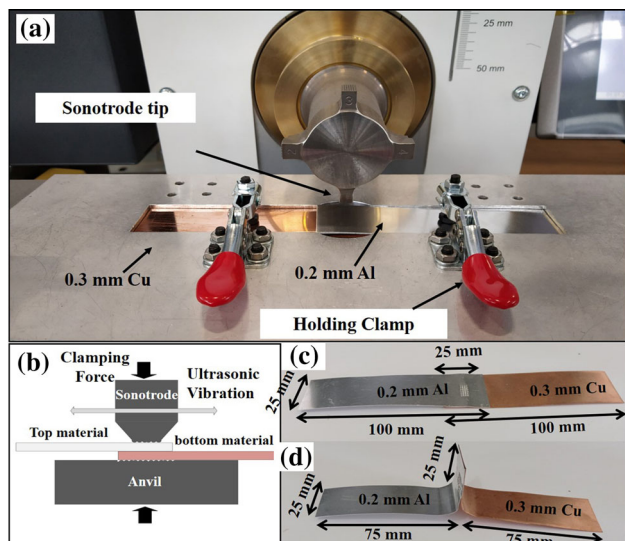
Fig. 1 Ultrasonic welding set-up and configurations (a) pictorial view of ultrasonic welding set-up head, (b) schematic of ultrasonic welding process, (c) and (d) lap shear configuration, and T-peel configuration respectively for Al-Cu joint

those on the horn were used to transfer the vibrating energy to the joining interface to create sound welds. Generally, the material with higher strength is used as the base material and the comparatively lower strength material is welded with the base material during the UW of two dissimilar ultra-thin sheet metals. Therefore, in the present work, Ni -coated steel and C101S were used as the base material for the Cu-Steel and Al-Cu material combinations, respectively.

The process sequence of the joining process followed in the present work is outlined as follows.

1. *Preparation of weld coupons* Weld coupons measuring 25×100 mm^2 were cut from sheets with a shearing machine. Their surfaces were cleaned with acetone to remove the dirt or foreign impurities that may hinder the joining process.
2. *Positioning of the sample in the UW machine* The samples were then placed between anvil and horn in two configurations a lap shear (Fig. 1(c)) and T-peel (Fig. 1(d)) configuration.
3. *Selection of process parameters* The process parameters were then set on the machine according to the experimental design and the welding process was carried out.

4. *Fabrication of welded samples* The welding of the ultra-thin sheets was carried out as per the selected parameters and welded samples were obtained.

2.4 Evaluation of Weld Properties

The quality of the weld obtained after the ultrasonic welding was evaluated by measuring the lap shear strength and T-peel strength expressed in terms of load bearing capacity (in N) of the joint. The test specimens for both configurations were prepared as per the DOE shown in Table 3. The prepared welded samples were tested on a uniaxial tensile testing machine (INSTRON 3367) having a maximum load bearing capacity of 30 kN. The tests were carried out at a cross-head speed of 2 mm/min for the lap shear samples and 20 mm/min for the T-peel samples. The load versus displacement data were recorded during the test for further evaluation. The obtained lap-shear and the T-peel loads of both the material combinations for different set of welding parameters is given in Table 3.

To identify the weld quality and to understand the joint mechanism, the metallurgical examinations of the weld were carried out with optical microscope and scanning electron microscope (SEM) of cross sections of the welded samples. The samples were first sectioned parallel to the welding direction using a high-speed precise abrasive cutter and then cold mounted using epoxy resin. Cold mounting was preferred as the hot mounting method involved high temperatures that might lead to change in the microstructure of the materials. The mounted specimens were then polished with SiC paper of varying grit diameters to remove material until the full sonotrode penetration depth was revealed. Thereafter, the specimens were polished with 9 μm and 3 μm diamond paste, followed by 0.05 μm colloidal silica solution with addition of hydrogen peroxide in order to obtain mirror surface finish.

The optical micrographs (up to 100x) of the weld region were acquired to visualize the flow of the material during the welding and the defects in the joining region. The SEM-EDS line scan was used to determine the material composition across the weld line with the help of ZEISS SIGMA FE-SEM. The micro-hardness measurements were taken by using fully automatic Buehler's Wilson VH1202 micro-hardness testing machine with 50 gm force (i.e., 0.49 N) and 10 s dwell time along the weld region to determine the change in microstructure of the material near the region. The temperature near the welded region was measured using a thermal camera in order to understand the change in the material behavior in ultrasonic welding. The above metallurgical characterizations were carried out for three categories of weld conditions, namely good-weld,

Table 3 Coded values according to CCD and the corresponding measured responses

	Coded values			Al-Cu		Cu-Steel	
Exp ID	P	T	A	Lap-shear, N	T-peel, N	Lap-shear, N	T-peel, N
1	−1	−1	−1	369.20	123.60	927.67	175.08
2	1	−1	−1	391.27	129.66	913.39	231.51
3	−1	1	−1	295.17	110.19	909.41	232.36
4	1	1	−1	194.77	104.41	862.69	221.16
5	−1	−1	1	268.69	113.12	891.83	232.45
6	1	−1	1	261.42	109.44	823.76	213.17
7	−1	1	1	297.43	106.96	845.22	208.66
8	1	1	1	252.44	102.17	714.19	241.97
9	−1.682	0	0	290.14	92.72	905.35	227.55
10	1.682	0	0	219.10	108.40	846.02	241.97
11	0	−1.682	0	369.01	132.13	900.68	224.03
12	0	1.682	0	290.93	103.76	893.40	218.17
13	0	0	−1.682	436.53	124.81	933.06	183.95
14	0	0	1.682	184.23	101.30	749.95	213.84
15	0	0	0	268.44	101.04	865.84	229.8
16	0	0	0	272.48	110.84	867.33	207.32
17	0	0	0	290.35	102.73	830.8	218.16
18	0	0	0	291.43	103.26	846.22	236.50
19	0	0	0	312.94	111.88	813.58	216.92
20	0	0	0	300.24	97.93	847.18	216.19

over-weld and under-weld. The over-weld condition referred to the weld obtained by the combination of the higher level of the parameters, and in this condition, the weld exhibited excessive softening of the material which resulted in maximum thinning in weld region and fracture was also observed. Similarly, the under-weld condition referred to the weld that was obtained at the combination of the lower limit of the parameters. This joint was characterized by insufficient joining which resulted in a weak joint. However, the weld obtained at the optimized parameters was termed as the good weld. The parameters for under-weld conditions considered were p=0.5 bar, t=0.15 sec and A=30 μm for Al-Cu joint and p=1.4 bar, t=0.21 sec and A=39 μm for Cu-Steel joint. Similarly, the parameters for over-weld condition were p=3.6 bar, t=0.65 sec and A=55 μm for Al-Cu joint and p=3.4 bar, t=0.65 sec and A=55 μm for Cu-steel joint. The good-weld condition referred to the optimum quality of the weld obtained in terms of the strength through the optimization technique and the parameters for good-weld were p=1.8 bar, t=0.21 sec, A=32 μm for Al-Cu joint and p=1.4 bar, t=0.64 sec, A=40 μm for Cu-steel joint.

3. Results and Discussion

3.1 Meta-Modelling Using RSM

The RSM method was used to identify the effect of process parameters on the lap shear and the T-peel strength responses. The stepwise polynomial regression model was used for the generation of RSM, because it was trackable and has a good predictive ability. In stepwise regression, the choice of predictive variables is carried out one at a time by considering F-test value. After all the variables are accounted, the model with best F-test value is chosen. In the study, the model terms were added and removed where the F-test value corresponding to significance levels threshold of 0.05. Different orders of polynomial equations were selected to fit the responses with the input parameters based on the experimental values of the responses. The higher order polynomial functions were selected over the lower order polynomial functions as the later were unable to estimate the fitness of the model accurately (Ref 15). In the present work, the quadratic models were chosen for fitting the Al-Cu F_{peel} and Cu-Steel F_{shear} responses, and these models were found significant based on the above tests. However, for Al-Cu F_{shear} and Cu-Steel F_{peel} response, the models were found not to be significant because of the large variation in the data. Thus, for the Al-Cu F_{shear} and Cu-Steel F_{peel} responses, cubic models were used to fit the responses with the input parameters. The validation of the generated model was carried out by determining and examining the different ANOVA parameters as shown in Table 4.

The R^2 value was observed to determine what percentage of responses were adequately explained. Along with these parameters, other plots and results were checked for the adequacy of the model. The notable parameters such as P-value, lack of fit, significant factors for both the responses and material combinations are also summarized in Table 4. Based on the selection criteria, the fitted models for the responses in terms of the input process parameters are shown as follows:

$$
\begin{aligned}
F_{shear(Al-Cu)} = {}& 6332.90 + 110.86 \times (p) - 1700.17 \times (t) \\
& - 397.94 \times (A) - 148.32 \times (p \times t) \\
& + 32.25 \times (t \times A) \\
& - 17.11 \times (p^2) - 567.90 \times (t^2) \\
& + 8.98 \times (A^2) - 0.07 \times (A^3)
\end{aligned} \tag{Eq 1}
$$

$$
\begin{aligned}
F_{peel(Al-Cu)} = {}& 326.59 - 331.12 \times (t) - 6.11 \times (A) + 2.85 \\
& \times (t \times A) + 201.47 \times (t^2) + 0.05 \times (A^2)
\end{aligned} \tag{Eq 2}
$$

Table 4 ANOVA parameters for the fitted models

ANOVA parameters	Responses	Al-Cu	Cu-Steel
Model P-value	Lap-Shear	< 0.0001	< 0.0001
	T-peel	0.0001	0.0003
Lack of Fit	Lap-Shear	0.6340	0.2413
	T-peel	0.3610	0.7676
R-Squared	Lap-Shear	0.9531	0.8398
	T-peel	0.8137	0.9706
Significant Factors	Lap-Shear	p, t, A, pt, tA, p^2 t^2, A^2, A^3	p, t, A, pA, t^2
	T-peel	t, A, tA, t^2, A^2	p, t, A, pt, pA, tA, p^2, t^2, A^2, ptA, p^2t, A^3

$$F_{shear(Cu-Steel)} = 962.08 + 259.76 \times (p) - 977.52 \times (t) \\ + 4.83 \times (A) - 6.39 \times (p \times A) + 986.43 \\ \times (t^2)$$

$$(Eq\ 3)$$

$$F_{peel(Cu-Steel)} = 6467.27 + 1167.73 \times (p) + 6078.97 \times (t) \\ + 290.84 \times (A) - 2782.06 \times (p \times t) \\ - 19.47 \times (p \times A) - 110.80 \times (t \times A) \\ - 45.25 \times (p^2) + 220.12 \times (t^2) \\ - 4.82 \times (A^2) + 41.54 \times (p \times t \times A) \\ + 160.52 \times \{(p^2) \times t\} + 0.03 \times (A^3)$$

$$(Eq\ 4)$$

3.1.1 Analysis of the Effect of Input Parameters on Responses. There were twelve 3D response surface combination images and four perturbation plots. For the visualization of response with respect to parameters, multiple levels of constant parameters were required to be considered which would multiply the numbers of 3D response plots. Therefore, only the required essential images of 3D response surfaces and perturbation plots obtained for the significant terms of Al-Cu joint and the Cu-steel joint are shown to visualize the parameters effects on responses in Fig. 2 and 3, respectively. In Al-Cu T-peel joint and Cu-steel lap shear joint, welding pressure and welding time, respectively, had no significant combined effects with other parameters as observed from the model (Eq. 2 and 3), also shown in Table 4. Therefore, for these two-joining combination, a 3D response surface was obtained for the parameters which had combined effects, and a perturbation plot includes all parameters was presented. The perturbation plot shows the effect of parameters on the response keeping the other parameters constant.

In case of the Al-Cu joint, the lap shear and the T-peel strength decreased with the increase in either of the amplitude or the welding time as depicted in Fig. 2. Moreover, with increase in welding pressure, the lap shear strength first increased and then decreased as can be seen from Fig. 2(a) and (b). However, welding pressure had no effect on T-peel strength as depicted in perturbation plot shown in Fig. 2(f). The decrease in both the output responses with increase in welding time and amplitude of sonotrode vibration can be attributed to the lower strength of the AA1050, and further increase in input energy, which is directly proportional to the welding time and amplitude of sonotrode vibration (Ref 19), decreases the thickness of the joint leading to the reduction in strength. The

higher energy input during the welding process makes the material softer because of the generated heat, and further applied pressure reduces the thickness of the joint. Therefore, when all the parameters were in their higher limits, the responses in terms of the strength of the weld were low for all the material combinations and configuration except for the peel strength for the Cu-Steel joint as observed from Fig. 2 and 3.

In the case of Cu-steel joint, the increase in parameters had negative effect on the lap shear strength keeping the other two parameters constant at the middle value (i.e., p=2.4 bar, t=0.425 sec, and A=47.5 μm) as observed in perturbation plot Fig. 3(b). However, the T-peel strength was found to be lower when all the parameters were at lower limit (i.e., p = 1.8 bar, t = 0.30 sec and A = 43 μm) as observed in Fig. 3(c) and (e). It is worthy to mention from the response surfaces and the perturbation plots that the input parameters had an ambiguous effect on the T-peel and lap shear responses. The reason for the difference is discussed further in the manuscript. Therefore, it is imperative to determine an optimized set of parameters that can either maximize both the responses simultaneously or make a trade-off between them. In order to carry out the optimization, the range of the parameters were set to the experimented range. However, for T-peel and lap shear response the objective was set to maximize the limit set to the highest and lowest responses observed during the experiment. A desirability value was calculated on the basis of the identified limit. The desirability value starts with zero at response below the lower limit and increases linearly to one upon reaching the higher limit. During optimization, a local maximum can be reached depending on the starting point of the optimization process. Therefore, the optimization process was carried out for hundred times, and the optimized parameters with a desirability value of one were selected. These optimum parameters were found in specific ranges, for example, the optimum input parameters for Al-Cu joints were found to be in the range of welding pressure (0.6-3.499 bar), welding time (0.15-0.295 sec), amplitude (30.024-35.331 μm). However, for the Cu-steel joint, the parameters were found in three distinct groups where, one input parameter was at the higher-range and the other two were at lower range compared to their experimental value as shown in Table 5.

It was difficult to select one set of parameters from the list of hundred optimized parameters which gives a local optimum. Therefore, a pareto-frontier curve was generated using the monte-Carlo technique. The pareto frontier curve is a balancing curve between the maximum lap shear and the T-peel loads. The points on this curve provide the optimal solutions, and it provides the flexibility to the design engineers to choose the optimal values of the loads based on the design criteria and the requirement of the strength of the joint. The generated Pareto-
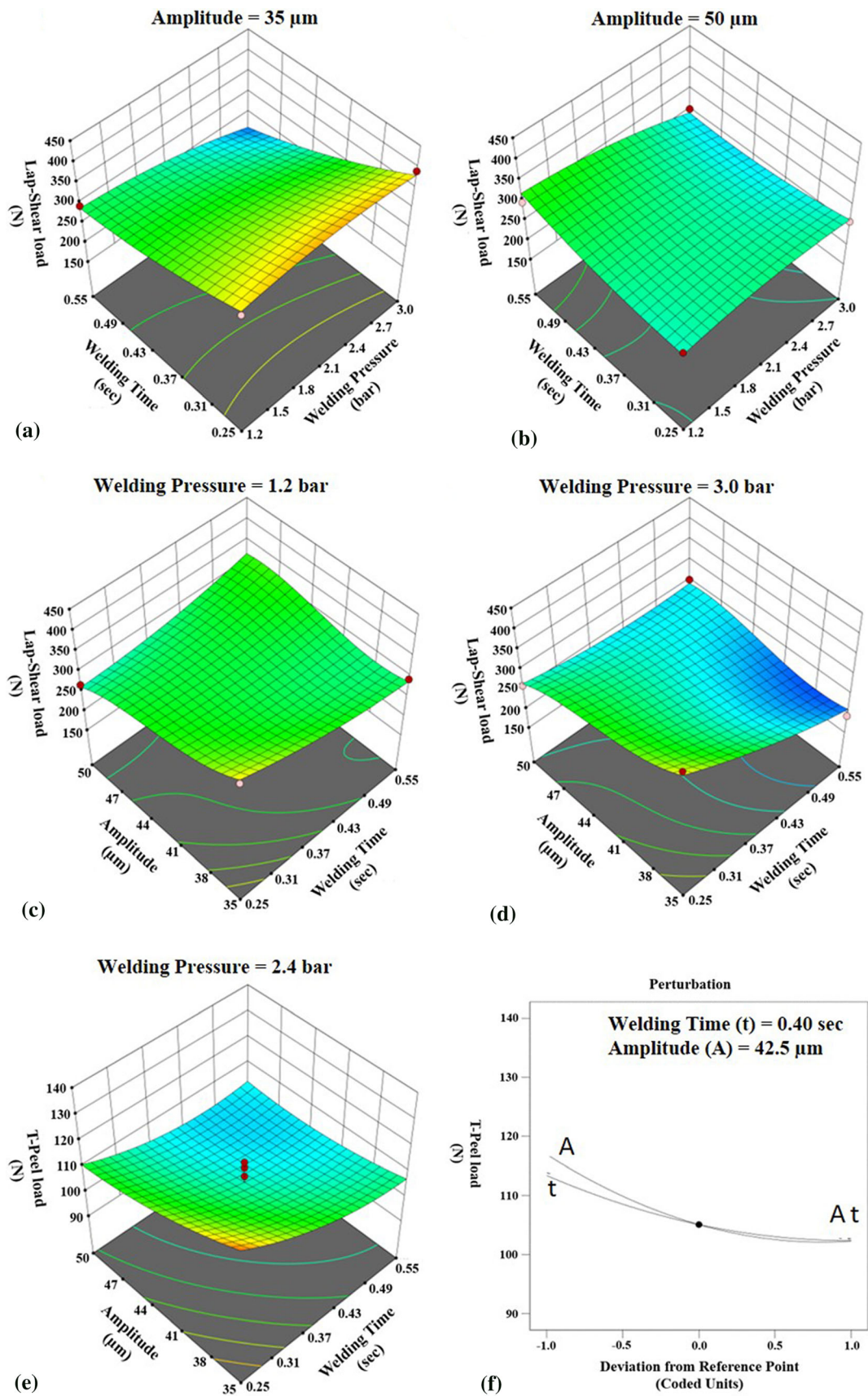
Fig. 2 Response surface of lap shear and response surface and perturbation graph of T-peel configuration for Al-Cu joint
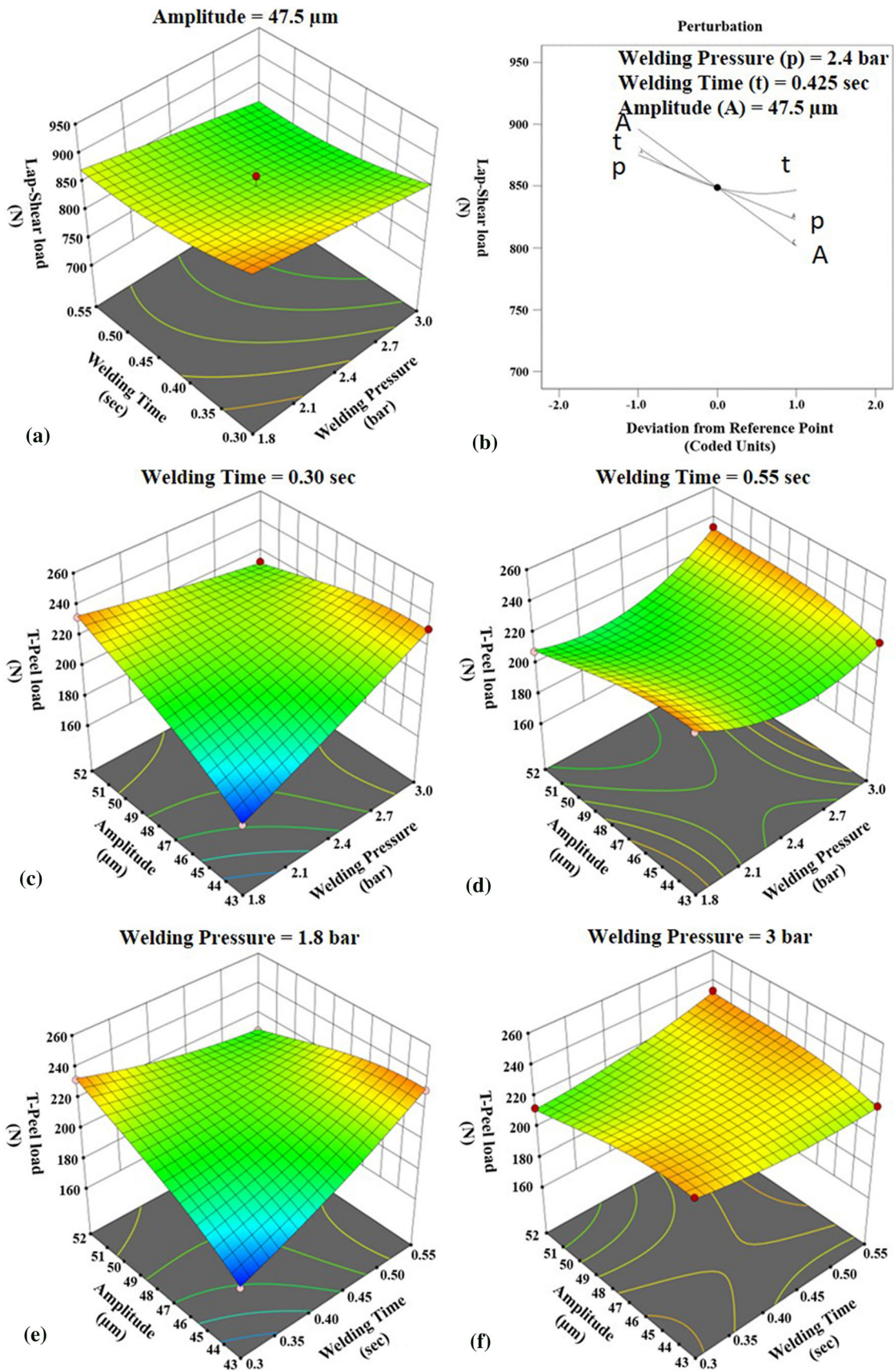
Fig. 3 Response surface and perturbation graph of lap shear and response surface of T-peel configuration for Cu-steel joint

Table 5 Identified groups of optimum input welding parameters for Cu-Steel joint

Group	Key feature	Welding pressure, bar	Welding time, sec	Amplitude, μm
Group 1	High Welding pressure	3.035-3.399	0.211-0.301	39.035-44.356
Group 2	High Welding time	1.395-2.000	0.607-0.649	39.008-42.089
Group 3	High Amplitude	1.395-1.624	0.210-0.220	51.150-54.551
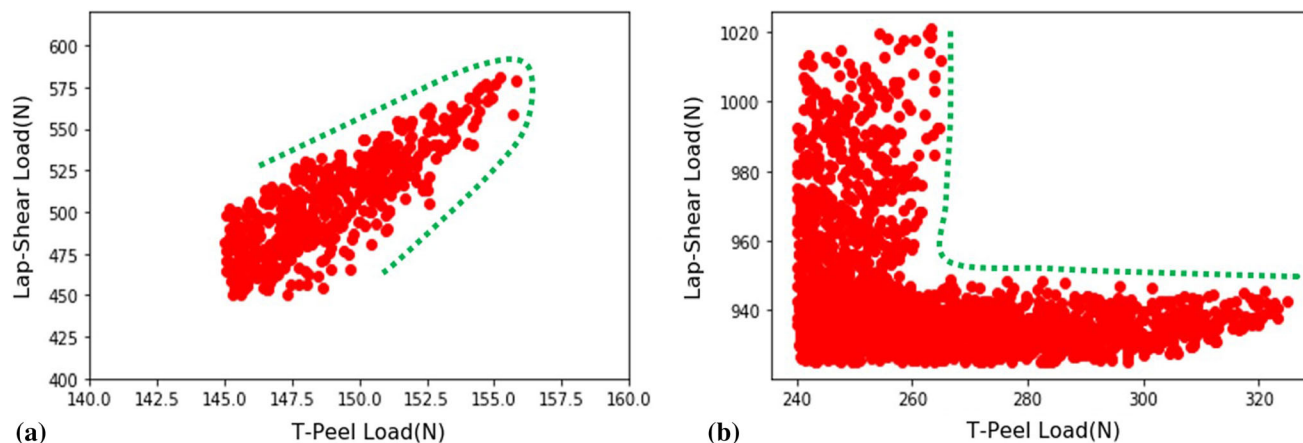
Fig. 4 Pareto-Frontier obtain from monte-Carlo method for the tread off between maximum lap shear and T-peel loads for (a) Al-Cu and (b) Cu-steel joint

Table 6 Confirmation of optimum process parameters

Joint Type	Group	Parameters			Predicted		Experimental		Error (%)	
		Welding pressure, bar	Welding time, s	Amplitude, μm	Lap-shear load, N	T-peel load, N	Lap-shear load, N	T-peel load, N	Lap-shear load, N	T-peel load, N
Al-Cu	N/A	1.87	0.18	33.9	453.39	144.18	431.24	145.90	5.1	1.2
	Group1	3.10	0.22	41	985.50	243.87	971.88	251.43	1.4	3.1
Cu-	Group2	1.81	0.64	41.5	980.22	280.76	952.81	279.79	2.8	0.01
Steel	Group3	1.4	0.21	54	941.85	281.38	932.58	281.29	0.01	0.01

frontier plots for both the lap shear load and the T-peel load for the Al-Cu joint and the Cu-steel joint are shown in Fig. 4(a) and (b), respectively.

In the Al-Cu joint, the peel strength and the lap shear strength were found out to be in the range of 140-160 N and 400-600 N, respectively. The variation of the range from the mean value that is the mid value of the range was 14% and 8% for the lap shear load and the T-peel load, respectively, and this variation was found throughout the entire input parameter domain. Similarly, for the Cu-steel joint, the values were in the range of 940-1020 N and 240-320 N for the lap shear and the T-peel joints, respectively, and a variation of 4% and 14% was found from the mean value for the lap shear and the T-peel load, respectively. The optimal solutions obtained for the Cu-steel joints were divided into three groups as per the unique feature of that group, and the same was also observed in case of the Pareto-Frontier curve. The lap shear load found above 1000 N corresponded to the optimal solutions present in group 1 with welding time between 0.211 and 0.23 s and amplitude between 39.035 and 39.30 μm. Similarly, the T-peel strength more than

300 N corresponded to the values present in the group 2 with the pressure value being below 1.5 bar, and the rest of the value of the load corresponded to the optimal solutions of the group 3. In order to validate the fitness of the model, three input parameter combinations were selected at random. For the Cu-steel joint, each parameter combination was created from one group. The selected parameters along with predicted and experimental values are shown in Table 6. It was found that the models were able to predict the lap shear and the T-peel load quite accurately with the maximum error in the prediction being under 6% and 4% for lap shear and T-peel loads, respectively.

3.2 Characterization of Ultrasonic Metal Welds

The optical micrographs of the samples for the three weld conditions obtained for both the material combinations i.e., Al-Cu and Cu-Steel are shown in Fig. 5. The sonotrode peak and valley regions can be very well observed from the obtained optical micrographs as shown in Fig. 5. It can be observed from Fig. 5 that maximum material thinning occurred near the sonotrode tip region i.e., the region near the weld, whereas the

thickness of the material at the valley region i.e., the region away from the weld was found to be higher than original thickness. Though similar kind of serrations were visible on the anvil, the variation in thickness in the substrate material was minimal because of its higher strength as compared to the joining material. Therefore, it can be inferred that during the joining process, the material flow took place from the sonotrode tip region to the valley region. This kind of material flow was higher in case of over-weld condition which led to excessive thinning of material at the weld region. The thinning can be accounted for higher welding time and amplitude in over-weld condition which led to the increase in the energy input, and further with higher welding pressure, the deformation of material increased. Contrary to the above phenomenon, in case of the under-weld condition, the energy input during the process and welding pressure was not sufficient enough to flow the material, and therefore, less thinning of material was observed near the weld region.
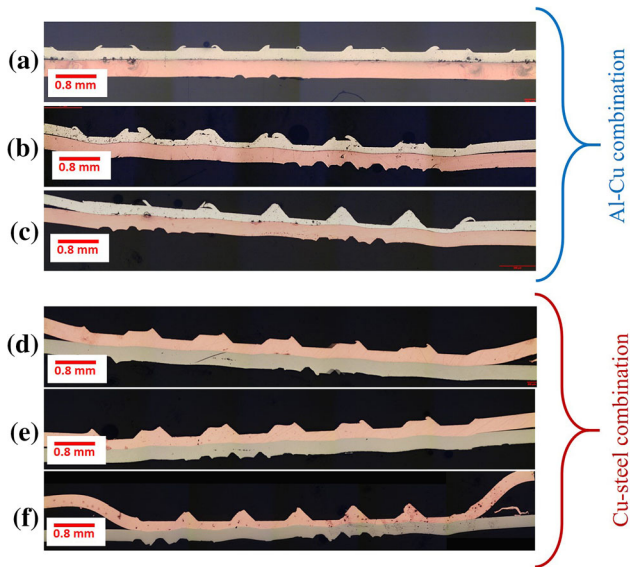
The higher magnification optical micrograph of the weld zone for both the material combinations is shown in Fig. 6. The application of pressure using the sonotrode tip on the top material led to the plastic deformation of the material, and the material started flowing in the upward direction to the valley region as shown in the figure with white arrow. Further, the presence of gaps near the weld region were observed in case of the under-weld condition as shown in Fig. 6, from which most of the gaps were observed in sonotrode valley region. This was because of the incomplete material flow in the case of under-weld condition. As in the under-weld condition, the energy and pressure were not sufficient to flow material to fill the gaps in valley region, which led lesser direct pressure at the valley region, resulting in less bonded region. Incomplete material diffusion was observed in some good-weld as shown in Fig. 6, whereas in over-weld complete material diffusion were observed as shown in Fig. 6 (over-weld).

These types of gaps are scarcely visible in case of the good and over-weld condition. However, excessive thinning was observed in over weld, which also resulted in a reduction in joint strength. The observed reduction in post-weld thickness for Al-Cu under-weld was up to 20% whereas for good-weld and over-weld, it was found to be around 50% and 60%, respectively. Similarly, in Cu-steel joint the reductions were 23%, 37%, and 53% for under-weld, good-weld, and over-weld, respectively. Similar observation was made before where the reduction in thickness in multi-layer Al-Cu joint was observed up to 70% (Ref 14). This was because in over-weld
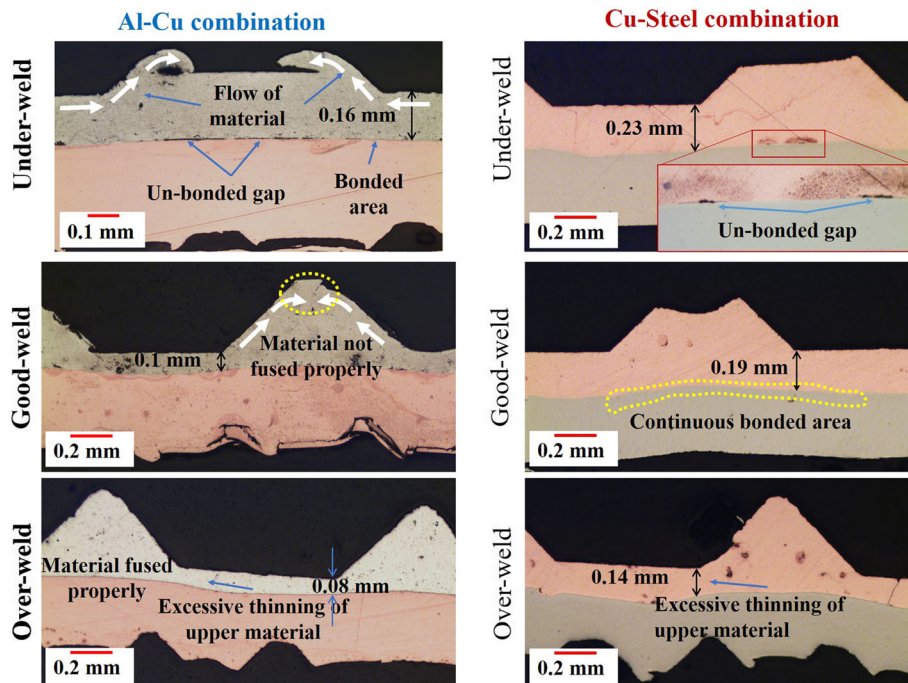

Fig. 5 Optical images of ultrasonic metal welds from Al-Cu and Cu-Steel combinations showing (a) Al-Cu under-weld, (b) Al-Cu good-weld, (c) Al-Cu over-weld, (d) Cu-Steel under-weld, (e) Cu-Steel good-weld, and (f) Cu-Steel over-weld

Fig. 6 Detailed features from under-weld, good-weld and over-weld condition

condition, higher energy was generated further leading to higher heat which made the material soft, simultaneously high-pressure from the sonotrode deformed the material.

3.2.1 Bond Mechanism. The mechanism of joint produced by ultrasonic welding process is derived from several theories which include (1) metallurgical adhesion because of a significant amount of plastic deformation (Ref 4, 5, 29, 30), (2) metal diffusion occurring across the weld interface (Ref 4, 5, 23), (3) melting confined to a particular location (Ref 4, 5, 23), and (4) mechanical interlocking (Ref 4, 5). The exact mechanism of joining of material through the UW process depends on the material combination and layers (Ref 28); therefore, a detailed analysis of it is necessary during the welding of ultra-thin dissimilar materials. During the welding process, the application of welding pressure generated a normal force on the joint, and the sonotrode vibration produced a shear stress near the weld zone (Ref 4, 8). The combined effect of both the above forces resulted in frictional heat which ultimately led to plastic deformation at the weld interface. The bonding proximity of the atoms increased due to the increase in temperature and pressure at the interface (Ref 8), thus leading to metallurgical adhesion and formation of micro-bonds observed in Fig. 7(a).

The gaps in the bonding region were negligible in case of the good-weld and over-weld conditions as can be observed from the optical images. The presence of lesser number of gaps in the welding region suggested that there was a substantial amount of formation of micro-bonds in this region. However, previously it was observed that a similar sequence of gaps and bonded region in good-weld and over-weld was generated at higher magnification (Ref 5, 9). The micro-bonds start to form and break in a continuous manner due to the sonotrode vibration during the welding process. With the progress in time, when the strength of the micro-bonds exceeds a threshold limit, the breakage of the bonds occurs because the vibration becomes minimal. Therefore, the bonding line begins to deform into a rolled and twisted shape called interfacial wave as shown in Fig. 7(c) and (d), and this twisted shape caused mechanical interlocking between the two materials as can be observed in

Fig. 7(b), (c) and (d) (Ref 5). Moreover, EDS line scan across the weld for good-weld condition i.e., the optimal condition, was conducted for both the material combinations as shown in Fig. 8. The inter-metallic diffusion can be observed clearly at the interface of the two dissimilar materials from the figure. However, the diffusion length which can be defined as the distance between two dark dotted line as shown in Fig. 8(c) and (d) was not the same throughout the overall weld region.

The diffusion length for the Al-Cu weld was ranging from 2 μm-10 μm, whereas, it was approximately 5 μm-20 μm for Cu-Steel joint. A hint of oxygen was also found in the weld during the SEM-EDS scan pointing to the fact that an oxide layer was formed in between the welding process. However, because of the generated compressive forces, abrasion due to the constantly vibrating sonotrode and galling effect, these oxide layers broke down and further supported the joining process (Ref 7). It can be concluded that the joint strength obtained in the present work was a combined effect of micro-bonds formed because of metallurgical adhesion, mechanical interlocking and inter-metallic diffusion. Thus, the process of bonding between the two dissimilar materials using the UW process can be summarized as (1) generation of normal and shear force along the weld line (2) continuous plastic deformation and flow of the material (3) the breakage of the oxide layer due to the compressive force, abrasion and galling effect and further, the removal of these due to excessive plastic deformation, and (4) formation of micro-bond at the high strain area and its growth along the weld line.

3.2.2 Work Hardening and Thermal Softening. Microstructural changes occur in the weld during the ultrasonic welding process because of the recrystallization due to extensive deformation at elevated temperature (Ref 4, 5, 19). In order to understand the hardening and softening of the material because of the welding process, microhardness measurements along the weld line were taken for both the material combinations and the three welding conditions. The measurements were taken on the top material as these materials
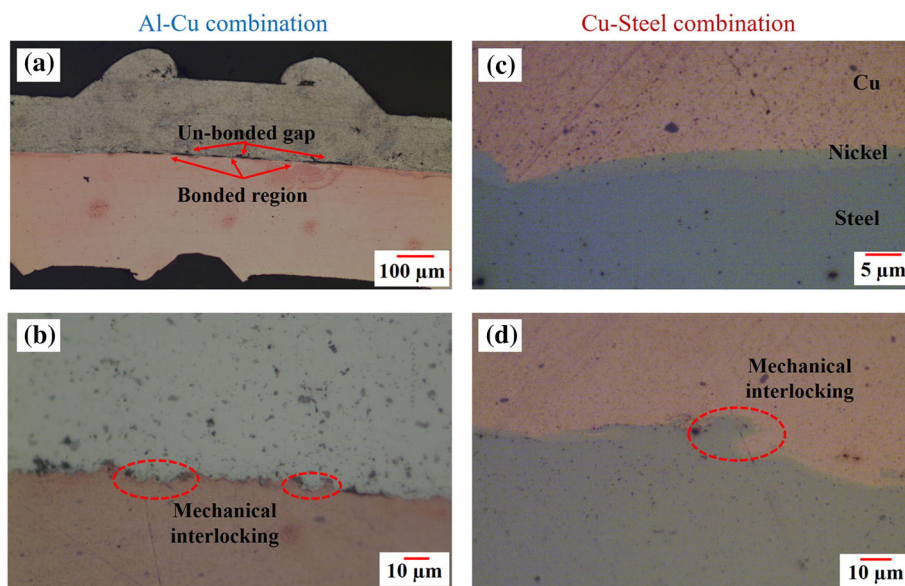

Fig. 7 Cross sectional view of the welded joints for Al-Cu joints (a) shows gaps in the joints and (b) mechanical interlocking, (c and d) for Cu-steel joint shows wave like material flow and mechanical interlocking
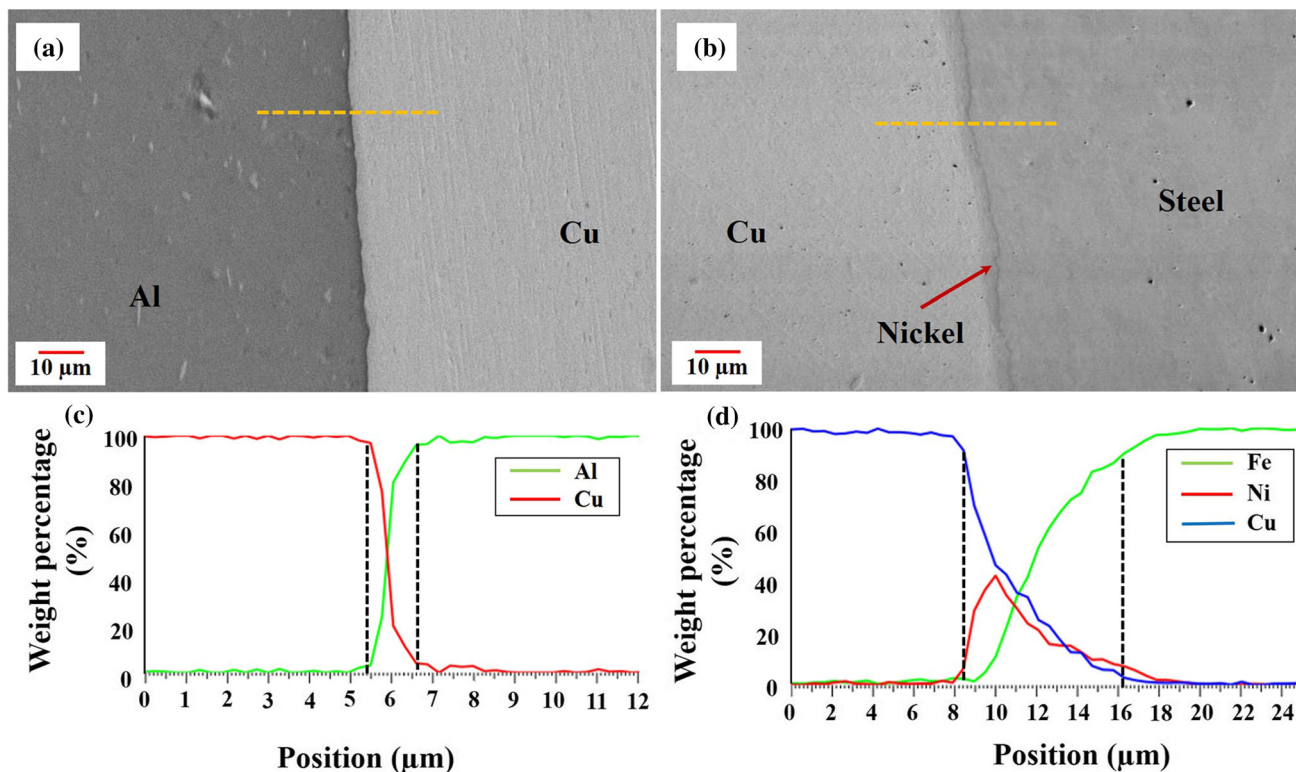
Fig. 8 SEM image and EDS line scan (a, c) Al-Cu joint and (b, d) Cu-steel joint
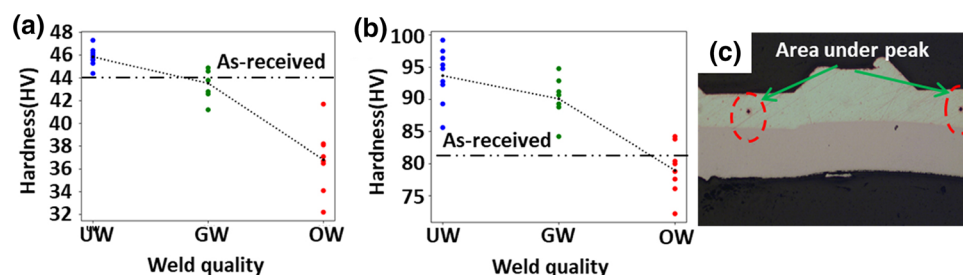

Fig. 9 (a), (b) Comparison of hardness for different welding conditions with hardness of as-received material for Al-Cu and Cu-Steel respectively and (c) location of hardness measurement taken under sonotrode peak

were comparatively softer than bottom material, therefore maximum material flow took place in the top material. The scatter plot depicting nine repetitions of the hardness compared with the as received ultra-thin sheets for all the three welding conditions is shown in Fig. 9(a) and (b), and the location of the hardness measurement taken is shown in Fig. 9(c). It was found out that in the Cu-Steel joint, there was an increment of approximately 17% in the hardness of the weld region as compared to the base Cu material for the under-weld condition, whereas it was around 5% in case of the Al-Cu joint when compared with the base Al material. For the over-weld condition, the hardness of the weld was found to be just below the hardness of the base Cu material for the Cu-steel joint, whereas a decrease of 5% in hardness was observed for the Al-Cu joints.

The decrease in the hardness below the hardness of the base material for the under-weld condition was because of the large amount of cold working involved during the welding process. It was also observed that the hardness was highest in the case of

under-weld condition, and it further decreased in the case of the good-weld and was minimum for the over-weld condition. This decreasing trend of the hardness in the three welding conditions was due to softening of the weld region because of the generation of the heat during the ultrasonic welding process (Ref 31).

In order to complement the trend of hardness observed for the three welding conditions, the temperature measurements were taken near the weld zone during the welding process. The plot of temperature with the progress of time of the weld region for Al-Cu joint and Cu-Steel joint is shown Fig. 10(a) and (b), respectively. The thermographic images at different position of joining of Cu-steel good welds were shown in Fig. 10(c), (d), (e) and (f). The measurement of the temperature at the exact welding zone was difficult during the ultrasonic welding process; hence, the temperature was measured with the help of infrared camera near the sonotrode tip region.

Two peak values of temperature were observed irrespective of the material combinations. The first peak value of temper-
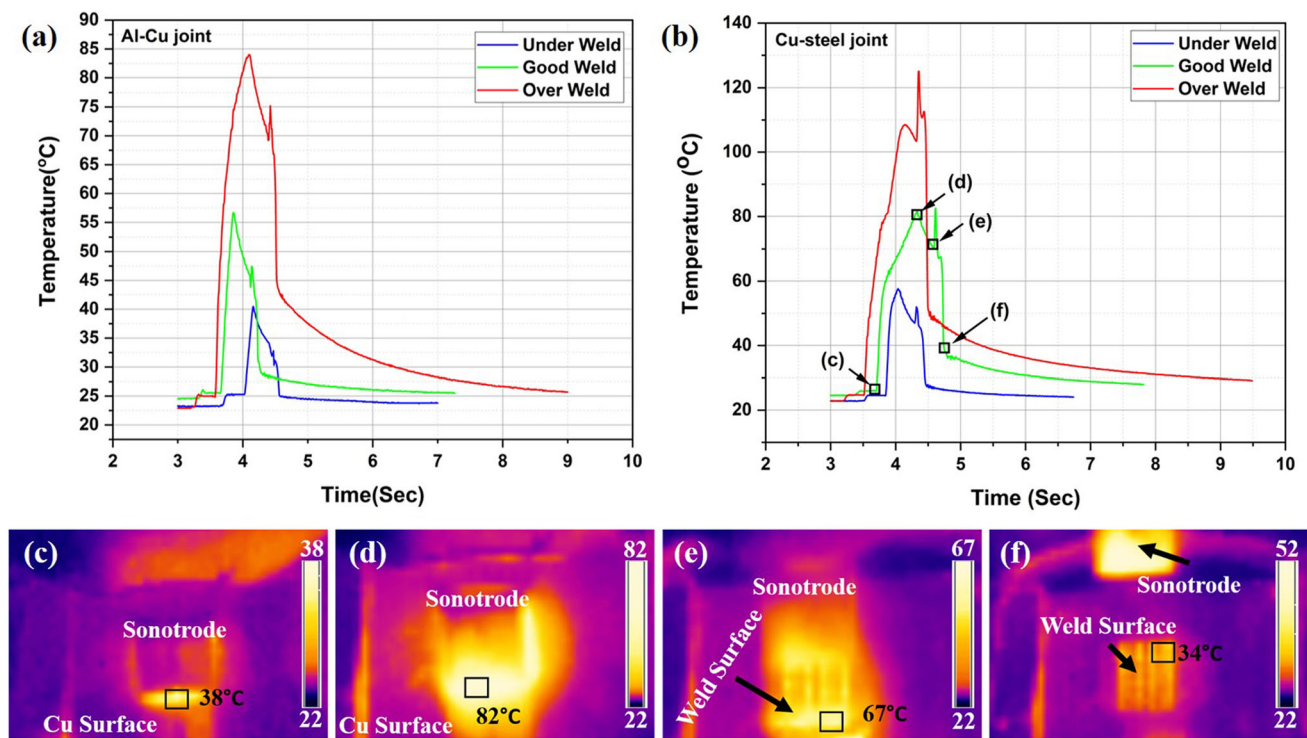
Fig. 10 Temperature profile for (a) Al-Cu, (b) Cu-steel joints during the welding and (c, d, e and f) the thermographic images obtained at different stages of the welding of Cu-steel good weld joint

ature of approximately 85 °C was observed in case of Al-Cu joint, whereas it was around 120 °C for the Cu-Steel joint. This peak temperature was achieved at the end of the joining process, and this temperature signified the temperature of the sonotrode tip at the weld interface. It was previously reported in the literature that the surface temperature generated during the ultrasonic welding process is at least 100°C lower than the interface temperature (Ref 32). Hence, it can be assumed that the temperature generated at the weld interface will be higher than the temperature measured at the sonotrode tip by an additional factor of 100 °C or more. Post the completion of the welding process, the sonotrode retracts itself, and the temperature can thus be measured at the surface of the formed weld. The temperature thus measured at this region and time signified the second peak in the temperature profile. The experimental setup was not able to measure the exact temperature at the interface as the optical inferred thermal imaging technique was used. However, it was able to show the pattern of heating and cooling during the welding, and hence, it can be inferred that due to the generation of heat, thermal softening was the predominant phenomenon for the change in the value of hardness along the weld line.

3.2.3 Evaluation of Hardness Profile. In order to understand the change in the strength of the weld, microhardness measurements were taken on the weld cross sections for both the material combinations in two directions (1) along the weld line i.e., the horizontal location and (2) across the weld line i.e., vertical location. The plot of variation of hardness along the weld line measured for peak and valley region of the sonotrode for both the material combinations is shown in Fig. 11(a) and (b). The hardness measurements were taken on the softer material with an offset of 0.1 mm from the weld line. The offset

was taken considering the gaps in bonding observed along the weld line in both the material combinations. In case of the under-weld condition, the hardness in sonotrode peak region was found to be higher than the valley region for both the material combinations. This was due to the plastic deformation of the material which initiated from the peak of the sonotrode tip and gradually shifted toward the valley area. Therefore, a higher amount of work hardening was observed in the peak area compared to the valley region. From Fig. 11, it was also observed that hardness at the valley area was close to the hardness of the as-received material. Therefore, it can be concluded that there was minimal work hardening in valley region, and further due to the softening of the material during the welding process, the hardness values became lower than the as-received material. However, in the case of good-weld, the hardness was nearly equal to the base material and for the over weld condition, the hardness was observed to be lower than the base material. The variation of hardness for the good-weld and the over-weld condition can be majorly attributed to the material softening because of the generated heat which was higher in case of over-weld condition, hence, the hardness of the weld decreased than the base material (Ref 4).

In order to complete the two-dimensional microhardness map, the hardness of the weld was measured across the joint as shown in Fig. 11(d) and (e). The measurements were taken in the valley area in two locations namely the surface and near the interface as depicted in Fig. 11(c). A similar trend was observed in case of the hardness measured across the weld line. Due to higher amount of plastic deformation and flow of material near the weld line, higher work hardening occurred near the interface as compared to the surface region. However, due to higher heat generation in case of good weld and over weld conditions, the hardness decreased due to material softening.
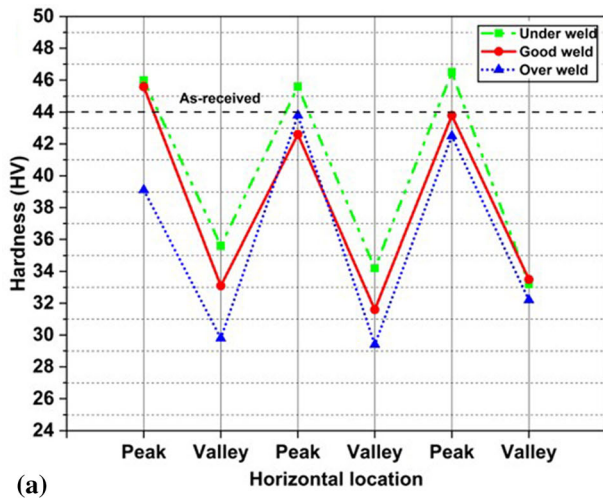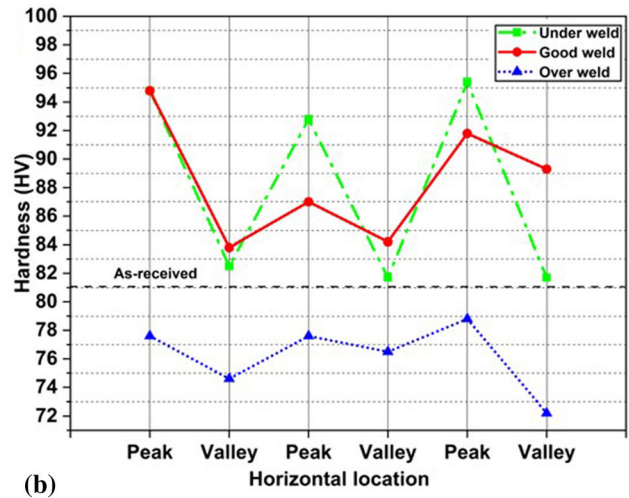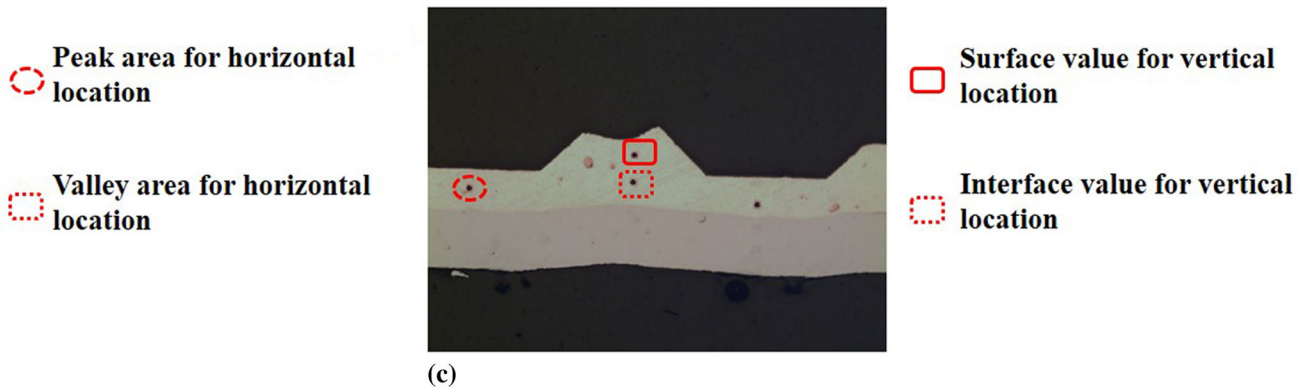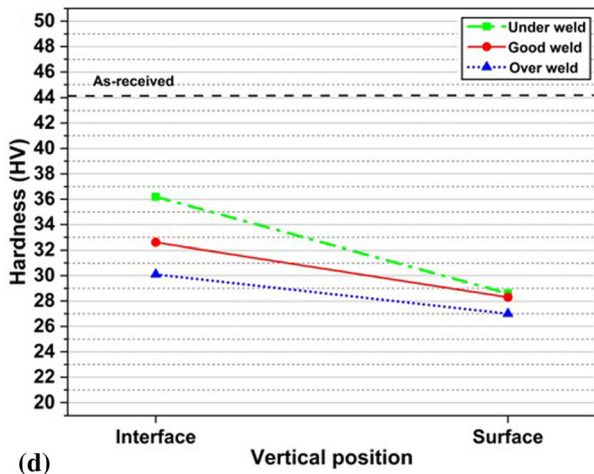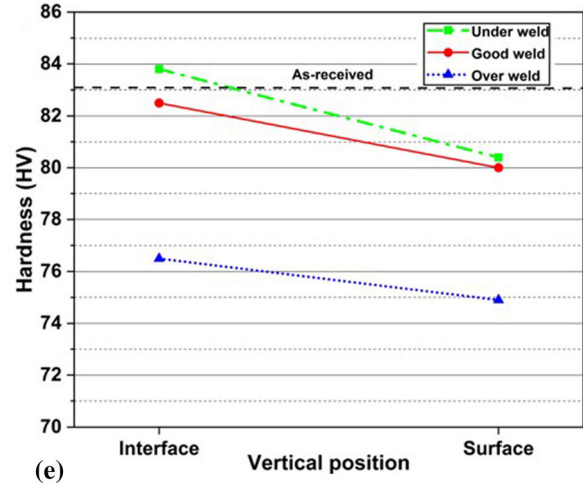
Fig. 11 Micro hardness distribution along (a) and (b) horizontal location for Cu-Steel and Al-Cu joint respectively, (e) and (d) vertical location for Cu-steel and Al-Cu joint respectively and (c) location of the hardness probe penetration

Hence, it can be concluded that in the ultrasonic welding process, initially work hardening occurs in the materials, and with gradual increase in the welding time, the temperature near the weld line increased which ultimately led to the material softening near that region (Ref 4, 5).

3.3 Failure Analysis of the Joints

The quality of the weld has been previously correlated with the properties of the weld such as the weld width, heat affected zone, penetration depth to width ratio (Ref 4, 5, 19). However, a very few attempts has been made in analyzing the failure mode occurring because of the physical attributes of the weld in the context of ultrasonic welding. The bond density and the post-weld thickness are the most important physical attributes that affect that weld quality in case of the ultrasonic weld. The relative bond density is evaluated by distinguishing the bonded and the unbonded region in the weld area and estimating the proportion of the bonded region with respect to the weld area. The post-weld thickness is defined as the thickness of the softer

material that is intended upon to the surface because of the pressure of the sonotrode. As mentioned in the literature, a good weld quality in reference to the ultrasonic welding must have a dense interfacial bond without excessive thinning of the material (Ref 4). It is noteworthy to mention that though gaps were scarcely visible in optical images of the weld cross section, the detailed fractography analysis of the weld area revealed the presence of many unbonded regions (Ref 22, 23). It was concluded from the microstructural analysis that the bond density was dependent on the input parameters such as the welding pressure, time and amplitude. It was observed that the bond density was minimum in case of under-weld condition, whereas it was higher for the over-weld condition and the good weld possessed an optimum value of the bond density (Ref 4). Apart from the bond density the post-weld thickness also affects the weld quality, and it was observed previously that the weld thickness was highest for the under-weld condition and lowest for the over weld condition.

Based on the above assumptions, an attempt was made to understand the mode and mechanism of failure of the welded joints in case of ultrasonic welding process. The different modes of failure were observed by the visual inspection of the tensile tested samples for both the joints. A typical case of failure in case of Cu-Steel joint for both the type of testing conditions is shown in Fig. 12. It can be observed that the failure occurred in the material primarily because of the interfacial separation and circumferential failure. The failure in case of the under-weld condition was a combination of partial circumferential failure along with interfacial separation for lap shear test, whereas it was only interfacial separation for the T-peel test. In case of the good weld condition, irrespective of the testing conditions, the material failure occurred through partial circumferential failure and material tear, whereas it was completely a circumferential failure for both the testing conditions for the over-weld condition.

Furthermore, a detailed analysis is presented in order to understand the mechanism of the failure and its relation with the physical attributes of the weld in case of ultrasonic welding process. It was assumed that the bond density and post-weld thickness were uniform throughout the weld zone, and all the
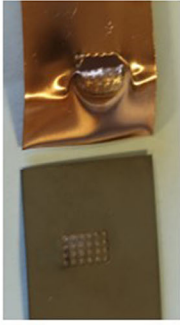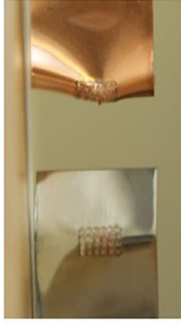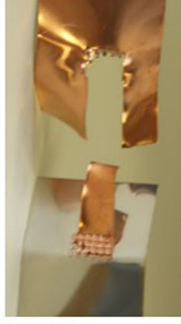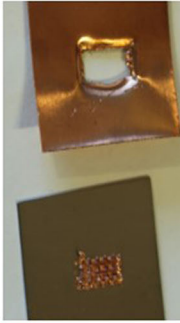

Fig. 12 Failure modes observed in lap shear and T-peel joint for Cu-steel material combination
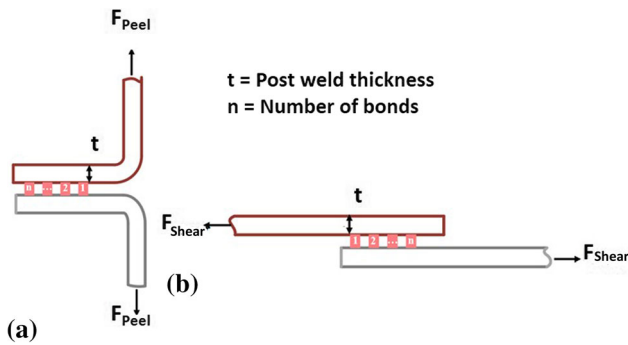
Fig. 13 Schematic of (a) T-peel joint and (b) lap shear joint showing a symmetric bond area

bonds formed within the weld area were of same surface area 'A_s' as shown in Fig. 13. The bond separation occurs when the strength of the bond is less than the force that is acting on the bond and the material fails when the strength of material at the region less than the force acting on it. It can be observed from the force analysis that the load in case of the lap shear tests is equally distributed among each bond, whereas each bond in case of T-peel test experiences equal amount of force. Therefore, in lap shear joint, the force acting on each bond can be calculated as F_{shear}/n, where n is the number of bonds and F_{shear} represents the maximum force that is acting on the joint. However, for the T-peel joints the bonds experience whole F_{peel} force with an additional momentum force, and hence the maximum force acting on a single bond can be defined by F_{peel} + Moment force, where F_{peel} is the maximum force that is being applied at the joint. Hence, the bond failure occurs more easily in case of the T-peel tests as compared to the lap shear test mode. In a similar manner, the post-weld thickness also determines the mode of failure of the materials in ultrasonic welding. Though the welded joint is subjected to an equal amount of force, if the post-weld thickness is higher, then the failure is more likely to be because of the failure of the bonds rather than the material failure. The similar kind of observation was made in case of the failure for both the testing conditions and the three welding conditions. The under-weld condition has lower bond density and higher thickness; hence the failure mode was mostly interfacial separation (bond failures) with a partial circumferential failure. However, in case of the over weld condition as the thickness of the welded joint was less, hence the failure occurred in the material through a complete circumferential failure. The failure in case of good weld condition can be either of the two basic modes of failure, and in the present study the material failed because of circumferential failure on the three sides and tear on the remaining side as can be observed from Fig. 12.

From the analysis it can be concluded that, comparing with lap shear joints bond failure are easier in T-peel joints. Therefore, higher bond density is important attribute for the T-peel joints than post-weld thickness which is complemented by observation in meta-modeling of Cu-steel joints as increase in parameters reduces the lap shear strength, whereas increases T-peel strength as shown in Fig. 3. The similar observations were also observed in the literature (Ref 28). However, in the case of Al-Cu joints, material tear was the predominant mode of failure in all welding conditions, due to low strength of aluminum.

4. Conclusions

The present work explored the applicability of the ultrasonic welding process for the joining of dissimilar ultra-thin sheet materials commonly used in battery applications. Two different material combinations i.e., aluminum (AA1050) – copper (C101S) and copper (C101S) – Ni-coated low carbon steel (Ni-steel) were used in order to investigate the weldability. The response surface methodology was used to optimize the important process parameters i.e., welding pressure, time and amplitude of vibration affecting the quality of the welding. The characterization of dissimilar joints and the mechanism of bond formation were explored through optical micrographs and SEM analysis. The major conclusions are summarized as follows.

It was observed from the response surface plots that in case of the Al-Cu joint, both the lap shear and the T-peel strength decreased with increase in either the welding time or amplitude. This can be attributed to the lower strength of Al compared to that of the Cu. In case of the Cu-steel combination, the lap shear strength decreased, whereas the T-peel strength increased for higher limit of the input parameters. This was because the higher limits of the input parameters caused higher energy and higher bond density which caused the reduction in post-weld thickness and in T-peel joint bonds failure is easier compare to a lap-shear joint for same input parameter values. The optimization of the good weldability region was carried out using the Pareto-Frontier curve for both the lap shear and T-peel loads for both the material combinations. The optimal lap shear and T-peel loads for Al-Cu were found to be in the range of 400 - 600 N and 140 - 160 N, respectively. Similarly, for the Cu-steel material combination, these loads were found to be in the range of 940 - 1020 N and 240 - 320 N, respectively.

The bonding mechanism of the ultra-sonic weld was studied for both the material combination, and it was found that the bonding strength was due to the combined effect of metallurgical adhesion, mechanical interlocking and intermetallic diffusion. It was concluded that the material underwent work hardening due to excessive plastic deformation, and a higher hardness was observed at the sonotrode peak area for all the welds. However, for over-weld condition, due to heat generation, thermal softening occurred near the interface resulting in reduced hardness value compared to the base material.

Conflict of interest

No conflict of interest exists in the submission of this manuscript, and is approved by all authors for publication. I would like to declare on behalf of my co-authors that the work described was original research that has not been published previously, and is not under consideration for publication elsewhere, in whole or in part. All the authors listed have approved the manuscript that is enclosed.

References

1. V. Dusastre and M. Armand, *Materials for Sustainable Energy: A Collection of Peer-Reviewed Research and Review Articles from*

Nature Publishing Group, Copublished with Macmillan Publishers Ltd, UK, 2010

2. A. Das, D. Li, D. Williams and D. Greenwood, Joining Technologies for Automotive Battery Systems Manufacturing, *World Electr. Veh. J*, 2018, **9**(2), p 22.

3. S.S. Lee, T.H. Kim, S.J. Hu, W.W. Cai and J.A. Abell, Joining Technologies for Automotive Lithium-ion Battery Manufacturing: A Review, *Int. Manuf. Sci. Eng. Conf. ASME*, 2010, **49460**, p 541.

4. S.S. Lee, T.H. Kim, S.J. Hu, W.W. Cai, J.A. Abell and J. Li, Characterization of Joint Quality in Ultrasonic Welding of Battery Tabs, *J. Manuf. Sci. Eng*, 2013 https://doi.org/10.1115/14023364

5. M. Shakil, N. Tariq, M. Ahmad, M. Choudhary, J. Akhter and S. Babu, Effect of Ultrasonic Welding Parameters on Microstructure and Mechanical Properties of Dissimilar Joints, *Mater. Des.*, 2014, **55**, p 263–273.

6. M. Brand, P. Schmidt, M. Zaeh and A. Jossen, Welding Techniques for Battery Cells and Resulting Electrical Contact Resistances, *J. Energy Stor.*, 2015, **1**, p 7–14.

7. C. Zhang and L. Li, A Coupled Thermal-Mechanical Analysis of Ultrasonic Bonding Mechanism, *Metall. Mater. Trans. B*, 2009, **40**(2), p 196–207.

8. X. Wu, T. Liu and W. Cai, Microstructure, Welding Mechanism, and Failure of Al/Cu Ultrasonic Welds, *J. Manuf. Process.*, 2015, **20**, p 321–331.

9. Y. Yang, G. Janaki Ram and B. Stucker, Bond Formation and Fiber Embedment During Ultrasonic Consolidation, *J. Matter Process. Technol.*, 2009, **209**(10), p 4915–4924.

10. Y. Zhao, D. Li and Y. Zhang, Effect of Welding Energy on Interface Zone of Al–Cu Ultrasonic Welded Joint, *Sci. Technol. Weld. Join.*, 2003, **18**(4), p 354–360.

11. Z. Zhang, K. Wang, J. Li, Q. Yu and W. Cai, Investigation of Interfacial Layer for Ultrasonic Spot-Welded Aluminum to Copper Joints, *Sci. Rep.*, 2017, **7**(1), p 1–6.

12. S. Elangovan, K. Prakasan and V. Jaiganesh, Optimization of Ultrasonic Welding Parameters for Copper-to-Copper Joints Using Design of Experiments, *Int. J. Adv. Manuf. Technol.*, 2010, **51**(1), p 163–171.

13. T. Kim, J. Yum, S. Hu and J. Spicer, Process Robustness of Single Lap Ultrasonic Welding of Thin, Dissimilar Materials, *CIRP Ann.*, 2011, **60**(1), p 17–20.

14. S. Dhara and A. Das, Impact of Ultrasonic Welding on Multi-layered Al–Cu Joint for Electric Vehicle Battery Applications: A Layer-wise Microstructural Analysis, *Mat Sci and Eng A*, 2020, **791**, p 139795.

15. K. Benyounis and A. Olabi, Optimization of Different Welding Processes Using Statistical and Numerical Approaches–A Reference Guide, *Adv. Eng. Softw.*, 2008, **39**(6), p 483–496.

16. K. Fujita and K. Yusuke, High-order polynomial response surface with optimal selection of interaction terms, 11th AIAA/ISSMO Multidiscip. Anal. Optim. Conf., 2006, 7054

17. P. Saha and D. Waghmare, Parametric Optimization for Autogenous Butt Laser Welding of Sub-millimeter Thick SS 316 Sheets Using Central Composite Design, *Opt Laser Technol*, 2020, **122**, p 105833.

18. A. Das, I. Masters and D. Williams, Process Robustness and Strength Analysis of Multi-layered Dissimilar Joints Using Ultrasonic Metal Welding, *Int. J. Adv. Manuf. Technol.*, 2018, **101**(1–4), p 881–900.

19. V.K. Patel, S.D. Bhole and D.L. Chen, Influence of Ultrasonic Spot Welding on Microstructure in a Magnesium Alloy, *Scr. Mater.*, 2011, **65**(10), p 911–914.

20. M.B. Shahid, S.C. Han, T.S. Jun and D.S. Park, Effect of Process Parameters on the Joint Strength in Ultrasonic Welding of Cu and Ni Foils, *Mater. Manuf. Process.*, 2019, **34**(11), p 1217–1224.

21. L. Xu, L. Wang, Y.C. Chen, J.D. Robson and P.B. Prangnell, Effect of Interfacial Reaction on the Mechanical Performance of Steel to Aluminum Dissimilar Ultrasonic Spot Welds, *Metall. Mater. Trans. A.*, 2016, **47**(1), p 334–346.

22. M.P. Satpathy and S.K. Sahoo, Microstructural and Mechanical Performance of Ultrasonic Spot-welded Al–Cu Joints for Various Surface Conditions, *J. Manuf. Process.*, 2016, **22**, p 108–114.

23. I. Gunduz, T. Ando, E. Shattuck, P. Wong and C. Doumanidis, Enhanced Diffusion and Phase Transformations During Ultrasonic Welding of Zinc and Aluminum, *Scr. Mater.*, 2005, **52**(9), p 939–943.

24. D. Chapman and T. Norris, Copper Development Association, https://copperalliance.org.uk/knowledge-base/resource-library/busbars-guidance design-installation, 2014

25. L. Pryor, R. Schlobohm and B. Brownell, A Comparison of Aluminum vs. Copper as used in Electrical Equipment, GE Consumer and Industrial, 2008, p 1-7

26. T. Takahashi, K. Ishizuka and K. Kawanishi, Properties of Nickel-Coated Steel Sheets for Battery Case, https://www.nipponsteel.com/en/tech/report/pdf/122-27.pdf, March 2015

27. C. Sudarsan, K.S. Prasad, S. Hazra and S.K. Panda, Forming of Serpentine Micro-channels on SS304 and AA1050 Ultra-thin Metallic Sheets using Stamping Technology, *J. Manuf. Process.*, 2020, **56**, p 1099–1113.

28. K. Bandyopadhyay, S.K. Panda and P. Saha, Optimization of Fiber Laser Welding of DP980 Steels Using RSM to Improve Weld Properties for Formability, *J. Mater. Eng. Perform.*, 2016, **25**(6), p 2462–2477.

29. H. Kreye, Melting Phenomena in Solid State Welding Processes, *Weld. J.*, 1977, **56**(5), p 154–158.

30. G.D.J. Ram, Y. Yang and B.E. Stucker, Effect of Process Parameters on Bond Formation During Ultrasonic Consolidation of Aluminum Alloy 3003, *J. Manuf. Syst.*, 2006, **25**(3), p 221–238.

31. S.I. Matsuoka and H. Imai, Direct Welding of Different Metals used Ultrasonic Vibration, *J. Mater. Process. Technol.*, 2009, **209**(2), p 954–960.

32. S. Elangovan, S. Semeer and K. Prakasan, Temperature and Stress Distribution in Ultrasonic Metal Welding—An FEA-based Study, *J. Mater. Process. Tech.*, 2009, **209**(3), p 1143–1150.